CLM-P882

CLM-P882

Aerodynamic aspects of a corona – preionised high repetition frequency excimer laser

Jim Fieret

CULHAM LABORATORY

AEA TECHNOLOGY

Aerodynamic aspects of a corona-preionised high repetition frequency excimer laser

Jim Fieret

Laser Technology Centre
AEA Technology, Culham Laboratory
Abingdon OX14 3DB
United Kingdom

Paper presented to OE LASE '90, Technical Conference on high Power Lasers, 14-19 January 1990, Los Angeles, Ca., USA.

Aerodynamic aspects of a corona-preionised high repetition frequency excimer laser

Jim Fieret

Laser Technology Centre
AEA Technology, Culham Laboratory
Abingdon OX14 3DB
United Kingdom

ABSTRACT

A compact high repetition rate XeCl excimer laser (CHIRP) has been developed for testbed purposes at Culham Laboratory. It features a novel gas flow circuit inside a single cylindrical pressure vessel which also encloses the discharge electrodes and centrifugal gas circulators. The average gas flow velocity in the laser cavity is 70m/s. The volume of the vessel ($0.25m^3$) has been minimized to reduce gas costs and otherwise be compatible with industrial shop-floor operation. A Mach-Zehnder interferometer and an image converter camera have been used to visualise discharge-induced shocks and waves in single shot mode. Three sources of shocks and waves have been identified. The first is at the plasma-gas boundary, where two shocks are created, one of which travels upstream and the other downstream through the gas flow duct. The second source is the thin sheath region near the cathode (i.e. the plasma-cathode boundary), which produces a transverse shock, travelling towards the anode. The third source is the mesh anode which produces a rarefaction wave followed by a compression wave, both travelling towards the cathode. Above the detection threshold of the present interferometer system (in the order of $(\Delta\rho/\rho)=10^{-3}$), density variations due to shocks and waves have been found in the discharge region up to 180 μs after the discharge.

1. INTRODUCTION

The work described here is an attempt to understand the generation and behaviour of discharge induced shocks and waves in a XeCl excimer laser with Helium as buffer gas. The experiments were carried out in single shot mode on a testbed XeCl excimer laser called CHIRP, within the EUREKA EU213 project. One of the aims of this Project is to develop a 1kW average power excimer laser.

The CHIRP laser was designed for operation at a PRF between 1 and 5kHz, at an output energy between 50 and 100 mJoule per pulse. For a given average laser power, high PRF minimizes the pulse peak power, thus imposing less thermal strain on cavity optics, output windows and other optical components in the beam path. High PRF can also reduce plasma generation in machining and enhance coupling efficiency in some non-thermal processes. However, high PRF operation requires a fast gas flow through the discharge region, and possibly additional facilities to attenuate shocks and waves.

The electrical pulser circuit of CHIRP consists of a thyratron-switched, low impedance transmission line, providing a prepulse and main pulse for the discharge[1]. The prepulse is isolated from the main pulse by means of a ferrite saturable magnetic inductor. Typical stored energy in this work was 2.5J for the main pulse at 10kV) and 2.5J for the prepulse (at 35kV).

The corona preioniser consisted of a saphire tube, enclosing a conductor, and is located behind the mesh anode. The preioniser is connected to a separate pulsed power supply.

The CHIRP testbed laser was designed to generate high gas flow velocities, but is also compact for low gas filling costs and industrial shop-floor compatibility[2]. The laser vessel has a volume of $0.25m^3$ and encloses the discharge electrodes and two centrifugal gas circulators which generate a gas flow velocity of 70m/s through the discharge region. Additional space for a heat exchanger and shock damping facilities is available within the vessel.

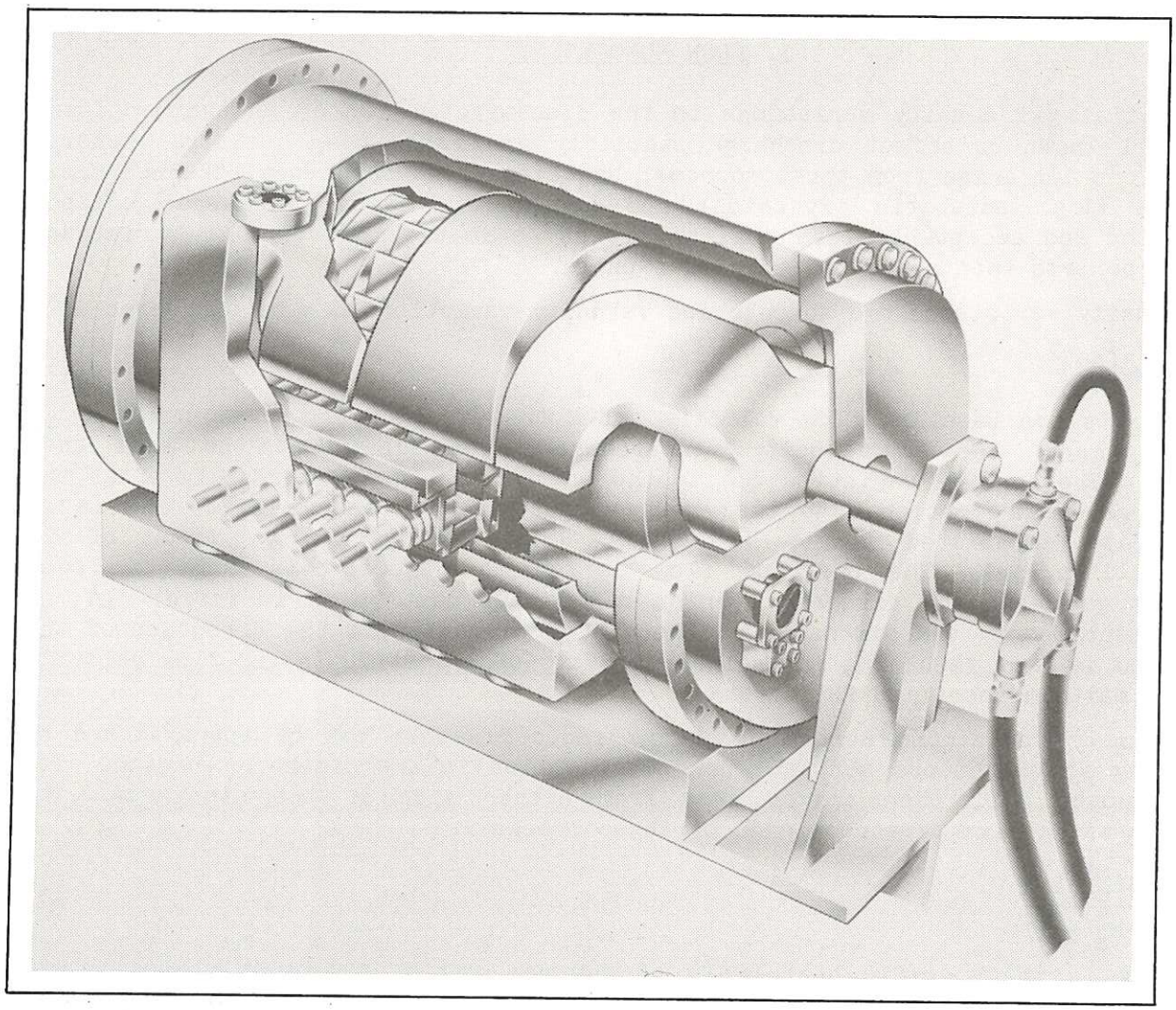

Figure 1. The CHIRP excimer laser.

2. BASELINE FLOW

Figure 1 shows the laser head, consisting of a stainless steel cylindrical pressure vessel closed by flat plates at either end. The laser cavity lies parallel to the axis of the vessel and each end plate contains an output window. The gas is circulated by two centrifugal fans on a single shaft. The flow velocity in the discharge region with ambient air was measured with a pitot tube and reaches an average of (55±10)m/s, at a circulator speed of 5400 rpm.

The gas flow velocity with Helium could be expected to be similar or better. This was confirmed with an interferometer and a framing image converter camera. The hot gas between the electrodes after a single discharge in Helium under a pressure of 1.1×10^5 Pa was observed for 200 microseconds. This is many times the duration within which the adiabatic expansion of the initial pressure pertubation is completed, so the latter does not contribute to the observed displacement. The measured flow velocity (averaged along the length of the discharge region) was (70±10)m/s, for a fan speed of 6000 rpm.

3. FLOW HOMOGENEITY

Spatial gas density variations in the discharge region of an excimer laser are well known to affect discharge stability and laser beam quality. Density variations can arise from three sources: baseline flow turbulence, thermodynamic effects (i.e. adiabatic expansion) and shocks and waves. For stable laser operation and acceptable beam quality, it is estimated that density variations $(\Delta\rho/\rho)$ be less than about 10^{-4} during a pulse.

Density variations due to baseline velocity variations can be expressed as[3]:

$$\frac{\Delta\rho}{\rho} = \frac{1}{2}M^2\left[\frac{\Delta u}{u}\right]^2 \qquad (1)$$

where u is the baseline flow velocity and M the baseline flow Mach number. In CHIRP, $(\Delta\rho/\rho)$ due to velocity variations are calculated to be less then 2×10^{-4}. The density variation due to the body of hot gas immediately after the discharge is proportional to the energy input in the laser medium, and is in this case calculated to be less than 0.25 for an energy input of 75 Joule/(litre.bar). The baseline flow serves to remove this body of lower density gas from the discharge region before the next pulse is fired. In the experiments here, the dimension of the discharge region in the direction of the gas flow is 5mm, resulting in a clearing ratio of 2.8 at 70m/s gas flow velocity at the maximum specified PRF of 5kHz.

Density variations across discharge induced shocks can be approximated by assuming a homogeneous spatial energy deposition in the discharge region. Two shock waves will then travel away from either side of the discharge. The density discontinuity across each of these shocks is:

$$\frac{\Delta\rho}{\rho} = \frac{2(M_S^2-1)}{2+M_S^2(\gamma-1)} \qquad (2)$$

where γ is the specific heat ratio of the gas and M_S the Mach number of the shock. For an energy input of 75J/(1.bar) in a XeCl laser with Helium as bulk gas, M_S can be calculated[4] to be approximately 1.07, and $(\Delta\rho/\rho)$ across the shock is approximately 0.11.

Density variations from shocks and waves can be present in the discharge region at the time of the next laser pulse, due to reflections. One source of reflections can be the body of hot gas from a previous pulse. If current return assemblies are present at either side of the discharge region, reflections off these can also occur.

4. SHOCKS AND WAVES

4.1 Methods

A Mach-Zehnder interferometer and a framing image converter camera were used to visualise shocks and waves in the discharge region, without baseline flow. The interferometer was used in zero-fringe mode, so that all intensity variations in the interferogram are due to density variations in the discharge region. A density variation of

$$\frac{\Delta\rho}{\rho} = \frac{\lambda}{(n-1)L} \qquad (3)$$

gave one fringe shift. λ is the wavelength of the interferometer light source (633nm from a HeNe laser) and n is the refractive index of the laser gas mixture at density ρ. L is the length of the laser cavity, which is 500mm in CHIRP. The experiments were carried out at a laser gas (Xe, HCl and Ne in Helium) pressure of $1.1\text{x}10^5$ Pa, at room temperature, so from formula [1] $(\Delta\rho/\rho)=2\text{x}10^{-2}$ per fringe. The minimum detectable variation was estimated to be in the order of $(\Delta\rho/\rho)=10^{-3}$. Some problems were encountered from ghost fringes from the imaging optics between the interferometer and the camera.

The framing image converter camera was used at a framing rate of 10^6 frames per second, with a fixed frame exposure time of 0.2μs. Ten consecutive full frames could be obtained in a single exposure. This meant that several exposures had to be taken to observe the discharge region over a time span of several tens of microseconds after the discharge. The repeatability of the discharge was good.

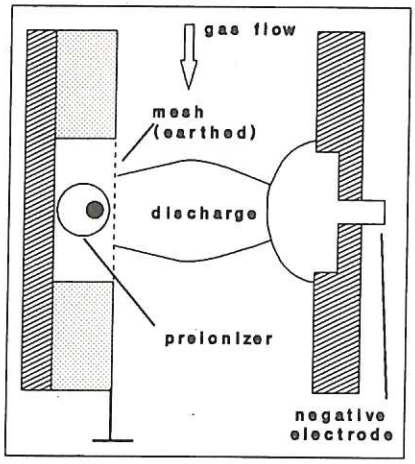

Figure 2. The discharge electrode assembly.

Figure 2 shows schematically the electrodes and preioniser. The anode is an earthed stainless steel mesh, with an open area ratio of 0.45 and circular holes of 60μm diameter. The saphire preioniser tube has an outer diameter of 9mm and is held in position behind the anode mesh. The gap between the mesh and preioniser is about 0.7mm. The total discharge energy storage was varied from 1.9 to 5.7J, by varying the main discharge capacitor charging voltage between 5 and 10kV and the prepulse charging voltage between 20 and 40kV. Power dissipation external to the discharge was estimated at 20%, corresponding to a discharge energy deposition of 25 to 75J/(l.bar) (at a reference temperature of 273K), at a total gas pressure of $1.1\text{x}10^5$Pa. The gas composition was He:Ne:Xe:Cl = 1000:21:19:1.

4.2 Results

Figure 3 shows the propagation of shocks and waves through the discharge region, for an energy load of 75 J/(l.bar). In each of the frames, the anode mesh is on the extreme left and the cathode on the right, as in figure 2. The weak circular patterns were caused by the imaging optics. The rapidly developing horizontal fringe pattern shows the expanding hot gas after the discharge has taken place.

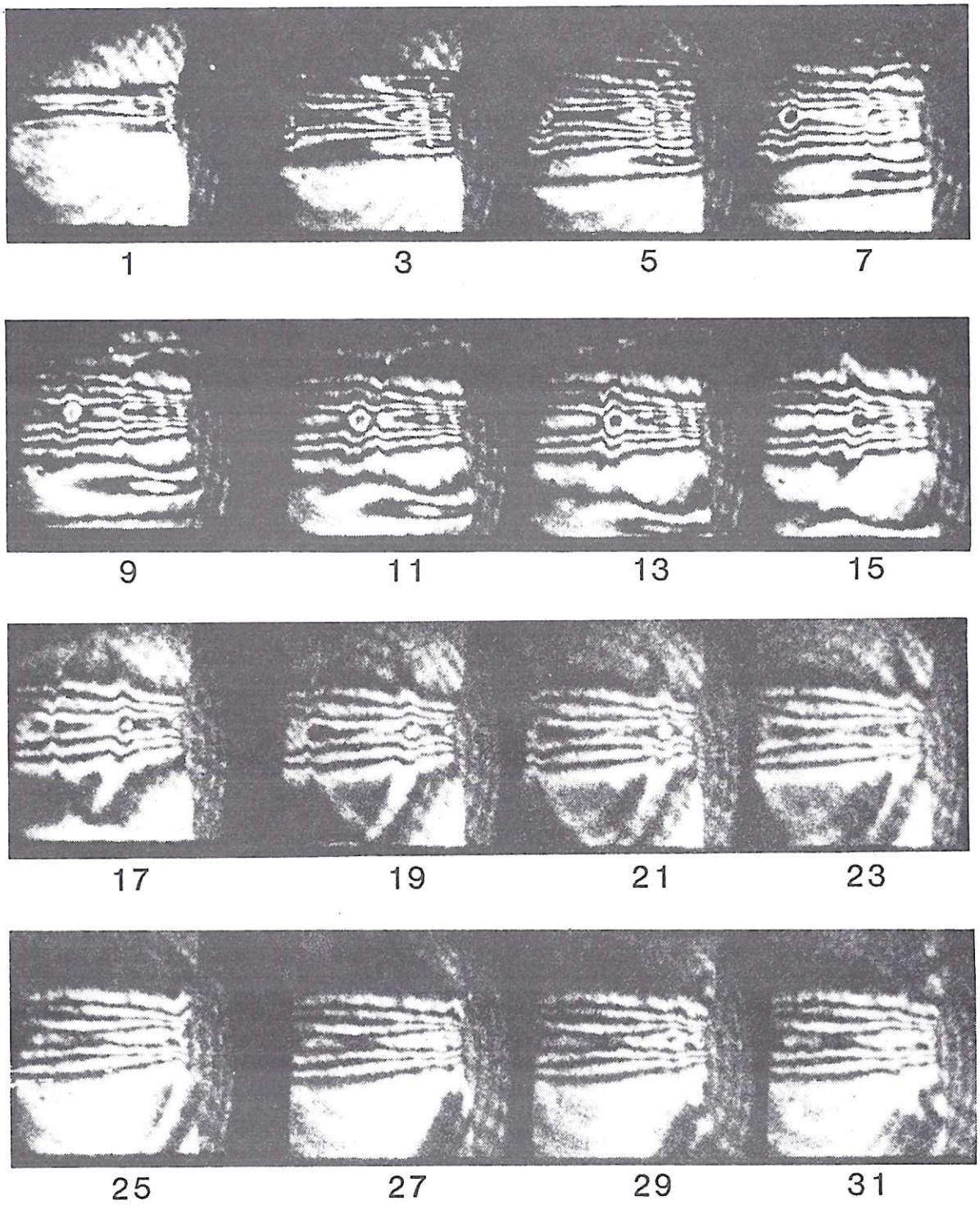

Figure 3. Shocks and waves in the discharge region for a discharge energy deposition of 75 J/(l.bar). Exposures are shown at 2μs intervals, starting at 1μs after the discharge.

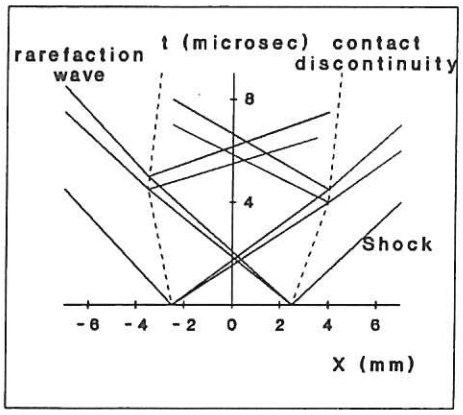

Figure 4. Longitudinal shocks and waves with baseline flow (70m/s). E=25J/(1.bar). Gas density and temperature change across the contact discontinuity.

The outer fringes on the top and base of the hot gas are two longitudinal shock waves, formed at the boundaries of the discharge. They travel up- and downstream into the gas flow duct. Expansion waves are also formed at the discharge boundaries and travel towards each other, where they can intersect, see figure 4. When the longitudinal shocks and waves have left the discharge region (after t=17μs), the remaining fringes show the body of hot gas, which must be removed from the discharge region by the the baseline flow. Gas density is lowest in the central region of the hot gas, and the density gradient is about 5 fringes, or $(\Delta\rho/\rho)\simeq 10\%$.

From t=5μs onwards, the fringes near the cathode on the right can be seen to converge sharply towards the horizontal centre line of the discharge region, showing a half-circular contour. This contour travels towards the left at approximately sonic velocity. The fact that the fringes are bent sharply towards the horizontal centre line of the hot gas means that a rapid compression is taking place. This can only be caused by a shock. As the shock passes through the gas, a more gradual expansion takes place, showing that the shock is a blast shock wave, in agreement with the general theory of thermal explosions[5]. The expansion 'tail' of the shock has in this case a length of about 2mm. The shock strength at t=7μs is about 0.5 fringe, or $(\Delta\rho/\rho)\simeq 1\%$. The shock weakens and its radius increases with time.

Also visible from t=5μs onwards is another fringe feature near the anode mesh on the left. This too has a half-circular contour. As the contour moves towards the right, again at approximately sonic velocity, the fringes first gradually diverge and then converge again. This must mean that the gas expands first, then suffers a compression. The separation between the expansion and rarefaction is approximately 1.5mm, or 1.5μs (the sonic velocity in the gas mixture is about 10^3m/s). These expansion and compression waves have a strength of $(\Delta\rho/\rho)\simeq 2\%$ each, at t=7μs, decreasing with time as their radii increase.

The shock from the cathode reaches the mesh anode opposite at t=23μs. No reflection can be observed. The expansion and compression waves from the anode reach the cathode at the same time. Reflection occurs from t=25μs to t=29μs. At t=46μs (not shown here) the wave combination has arrived back at the anode mesh, where no further reflection is observed.

New pertubations enter the discharge region about 100 to 180 μs after the discharge has taken place (not shown here). These variations have a magnitude of $(\Delta\rho/\rho)\simeq 2\%$ and are thought to be longitudinal waves, reflected off the current returns on either side of the discharge region. The time delay between the discharge and the reflected waves is consistent with the distance of 60mm between the current returns and the discharge boundaries.

Figure 5 shows the behaviour of shocks and waves for discharge energy loads of E=50, 40, 30 and 25J/(l.bar). The density variations become smaller as E decreases, but the shock from the cathode and the expansion/compression waves from the anode are still observed.

The shock originating at the cathode is thought to result from the large amount of energy deposited into the cathode sheath region during the discharge, resulting in a locally higher temperature then the rest of the discharge.

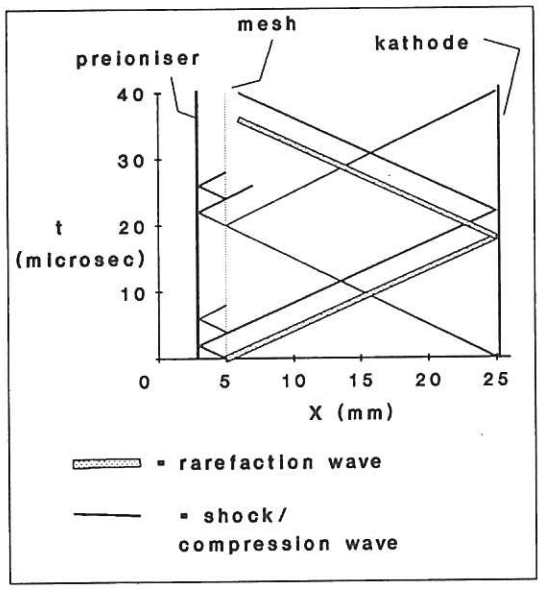

Figure 6. Transverse shocks and waves in the discharge region.

The expansion and compression waves originating at the anode mesh are due to the pressure gradient across the mesh, immediately after the discharge. To the right of the mesh the gas is heated up by the discharge, while the gas on the left is not heated. This results in a shock wave travelling away from the mesh towards the left, compressing the cold gas, and an expansion wave travelling towards the right, into the discharge region. The shock can reflect off the preioniser, traverse the mesh and continue its path into the discharge region, behind the expansion wave. It is possible that the mesh reduces the steepness of the shock, resulting in a more gradual compression wave. This explanation is consistent with the distance between the compression and expansion wave, which is approximately twice the distance between the mesh and the preioniser bar. Figure 6 shows the course of events in a position vs. time diagram.

CONCLUSIONS AND DISCUSSION

The CHIRP excimer laser has proved that a small, compact design is capable of delivering a high baseline flow velocity of 70m/s through the discharge, with good homogeneity ($\Delta\rho/\rho$ less than 2×10^{-4}), using Helium as buffer gas.

At an energy deposition between 25 and 75J/(l.bar), three sources of shocks and waves have been identified. Longitudinal shocks are formed at the discharge boundaries, travelling up and down stream into the gas flow duct. A transverse shock is created at the cathode sheath region, and the anode mesh is the source of an expansion wave followed by a compression wave 1.5μs later. Transverse shocks can reflect off the cathode, but no reflections off the anode mesh have been observed. It is possible that the mesh has a damping and scattering effect on waves, and that reflections are too faint to detect with the present system. Further experimental evidence is neccessary with improved interferometer sensitivity.

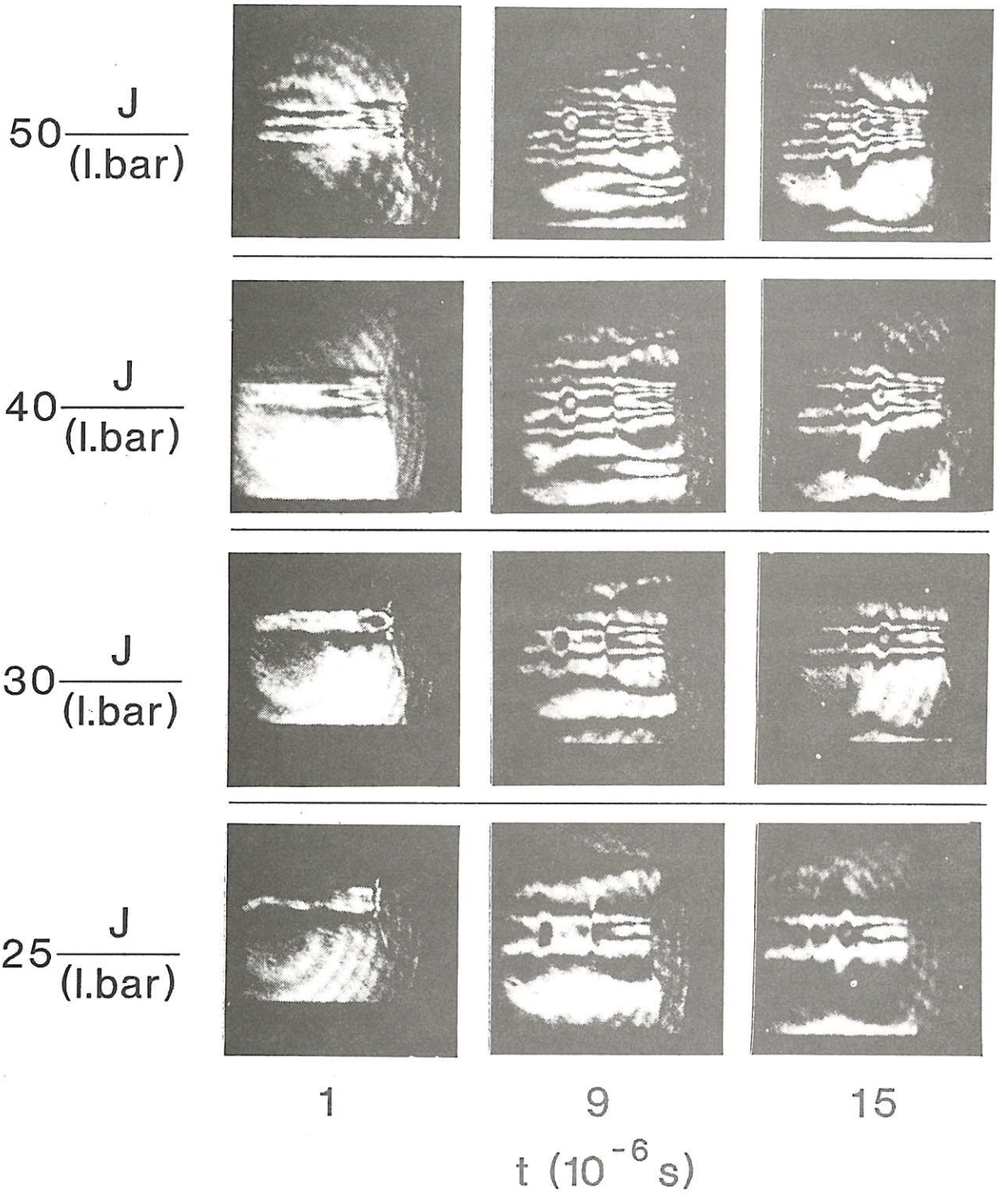

Figure 5. Transverse shocks and waves in the discharge region, for various energy densities in the discharge. Exposures are shown at 1, 9 and 15μs after the discharge.

The results here suggest that longitudinal shocks could be be a limit to the maximum PRF, and it may be necesary to employ shock damping techniques. However, Fontaine e.a.[6] have described experiments on a high PRF XeCl excimer laser with Neon as buffer gas and an energy deposition of 115J/l at 2200mbar pressure (about 50J/[l.bar]).
With shock dampers present in the laser, the PRF seemed to be limited not by shocks but by phenomena related to the heating of the electrodes.

In the CHIRP excimer laser, transverse waves decay to below $\Delta\rho/\rho \approx 10^{-3}$ within 46μs, and longitudinal waves, reflected off the current returns, are present up to 180μs after the discharge has taken place. The question remains whether $\Delta\rho/\rho=10^{-3}$ is low enough to ensure a stable discharge. For good laser beam quality, a figure of $\Delta\rho/\rho<10^{-4}$ is generally quoted[3] for Helium based laser mixtures, and this is assumed to be sufficiently low for stable discharge operation.

Future work on the CHIRP laser will include an assessment of the effects of shocks and waves on maximum PRF, using an interferometer visualisation system with improved detection threshold. Special attention will be given to longitudinal shock reflections, occuring at the current returns, gas flow duct and possibly at the body of hot gas from the previous pulse. Investigations of the later will be assisted by a one-dimensional code[7] for the simulation of longitudinal shock generation and propagation in the CHIRP laser.

ACKNOWLEDGMENTS

This work was funded by the EU213 EUREKA project, and by the AEA Technology Underlying Research programme. The author thanks Dr. MK Bevir, Dr. JM Green for useful discussions, R Heath, MA O'Key, Dr. MR Osborne, AFDS Taylor and Dr RJ Winfield (all at Culham Laboratory), for help and advice during the experimental programme.

REFERENCES

1. RJ Winfield, JM Green, J Fieret, K Hawkins, R Heath, MR Osborne, E Stuart and AFDS Taylor, 'Pulse power for the CHIRP XeCl laser', SPIE Vol. 1046 'Pulse Power for Lasers II', 1989, pp98-105.

2. J Fieret, United Kingdom Patent Application no. p89-05937, March 1989.

3. CC Shih and CM Charles, 'Gas dynamic and acoustic management for visible wavelength lasers', SPIE Vol. 138 'Advances in Laser Technology (Emphasizing Gaseous Lasers)', 1978, pp75-82.

4. Ed. GK Batchelor, 'Notes on the dynamics of shock-waves from bare explosive charges', in: 'The scientific papers of Sir Geoffrey Ingram Taylor', Vol. 3, Cambridge University Press, Cambridge (1963), pp255-59.

5. WE Baker, 'Explosions in air', University of Texas Press, Austin and London (1973), ISBN 0-292-7200-3.

6. B Fontaine, B Forestier, Ph Delaporte and P Canarelli, 'Pulse repetition frequency effects in a high average power X-ray preionised excimer laser', SPIE Vol. 1132 'High power lasers and laser machining technology', 1989, pp64-72.

7. A Thyagaraja and DF Fletcher, 'CUDGEL: A one-dimensional transient simulation of excimer laser gas dynamics', Culham Laboratory Report no. CLM-R297 (1989), ISBN 085311 1812.